—For Table of Contents Use Only—

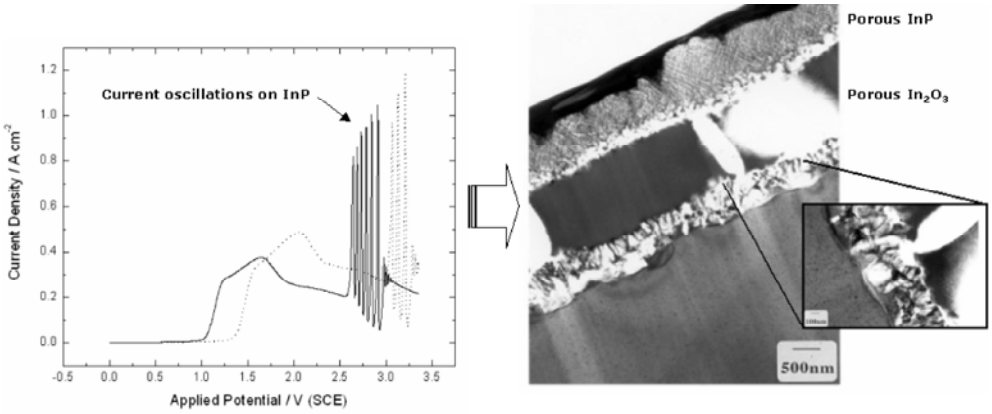

Manuscript title: **Simultaneous observation of current oscillations and porous film growth during anodization of InP**

Authors: C. O'Dwyer, D. N. Buckley and S. B. Newcomb

Simultaneous observation of current oscillations and porous film growth during anodization of InP

C. O'Dwyer[†‡], D. N. Buckley[†] and S. B. Newcomb[*]

[†]*Materials and Surface Science Institute, University of Limerick, Ireland*

[‡]*Tyndall National Institute, Lee Maltings, Cork, Ireland*

[*]*Sonsam Ltd., Glebe Laboratories, Newport, Co. Tipperary, Ireland*

Abstract

The observation of spontaneous oscillations in current during anodization of InP in relatively high concentrations of KOH electrolytes is reported. Oscillations were observed under potential sweep and constant potential conditions. Well defined oscillations are observed during linear potential sweeps of InP in 5 mol dm^{-3} KOH to potentials above ~1.7 V (SCE) at scan rates in the range 50 mV s^{-1} to 500 mV s^{-1}. The oscillations observed exhibit an asymmetrical current versus potential profile and the charge per cycle was found to increase linearly with potential. More complex oscillatory behavior was observed under constant potential conditions. Periodic damped oscillations are observed in high concentrations of electrolyte whereas undamped sinusoidal oscillations are observed in relatively lower concentrations. In both cases, anodization of InP results in porous InP formation and the current in the oscillatory region corresponds to the cyclical effective area changes due to pitting dissolution of the InP surface with the coincidental growth of a thick porous In_2O_3 film.

I. INTRODUCTION

At present, there is much interest in the electrochemical formation of photonic crystals and their potential applications. Such photonic crystals have been produced using electrochemically formed porous Si. However, it has been observed that the formation of porous layers and films are accompanied by oscillations in either potential or current under certain conditions. Although oscillatory behavior has been reported for metal anodes under a variety of conditions in many electrode/electrolyte systems [1–6], there have also been numerous reports of oscillatory behavior during the anodization of semiconductor electrodes in aqueous solution. Oscillations have been observed during the anodization of p-type [7–10] and n-type [11–13] silicon electrodes mainly in fluoride containing electrolytes. The oscillations are typically observed in the electropolishing region of the applied potential where a thin surface film is present [14]. Evidence for the cyclic growth and dissolution of thin SiO_2 layers on the silicon surface during the oscillatory regime was also reported [15, 16]. The shape, frequency and duration of the oscillatory behavior were reported to be dependent on electrolyte composition, temperature, applied anodic current density and crystal orientation of the substrate. Several hypotheses have been proposed [17, 18], but as yet, no general mechanism has been advanced that explains all of the reported results. Recently, oscillatory behavior has been reported on n-InP electrodes under anodic conditions [19, 20]. These voltage oscillations were reported to be linked to the synchronous lateral modulation of the pore diameter during anodization [21]. Although many reports of porous InP formation under a variety of anodization conditions have been previously reported [22–24], electrochemical current oscillations that simultaneously accompany porous InP formation and porous anodic film growth has not been observed until now.

In this paper, we report on the first observation of anodic oscillatory behavior with the simultaneous formation porous InP and the subsequent growth of a porous anodic film at the semiconductor-electrolyte interface. The characteristics of current oscillations observed during the anodization of InP electrodes in KOH are presented and compared with previous observations of film growth and porous layer formation under different conditions.

II. EXPERIMENTAL

Working electrodes consisted of polished (100)-oriented monocrystalline sulfur doped n-InP with a carrier concentration of approximately 3×10^{18} cm^{-3}. An ohmic contact was made by alloying indium to the InP sample and the contact was isolated from the electrolyte by means of a suitable varnish. Anodization was carried out in aqueous KOH electrolytes with concentrations in the range 2−5 mol dm^{-3}. A conventional three electrode configuration was used employing a platinum counter electrode and saturated calomel reference electrode (SCE) to which all potentials are referenced. Prior to immersion in the electrolyte, the working electrode was dipped in a 3:1:1 H_2SO_4:H_2O_2:H_2O etchant to remove the native oxide and any orgnic contaminants and rinsed in deionized water. All of the electrochemical experiments were carried out at room temperature and in the dark. A CH Instruments Model 650A Electrochemical Workstation interfaced to a Personal Computer (PC) was employed for cell parameter control and for data acquisition (1000 samples s^{-1}). Cross-sectional slices were thinned to electron transparency using standard focused ion beam milling procedures [25] by means of a FEI 200 FIBSIMS workstation. Scanning electron microscopy (SEM) was performed using a JEOL JSM 840 and the transmission electron microscopy (TEM) characterization was performed using a JEOL 2010 TEM operating at 200 kV.

III. RESULTS AND DISCUSSION

Linear potential sweeps were acquired at a series of scan rates in the range 50 mV s^{-1} to 500 mV s^{-1}. Typical current density versus potential curves for n-InP electrodes are shown in Fig. 1. In Fig. 1a, the potential was scanned at a rate of 300 mV s^{-1} from an initial potential of 0.0 V to an upper potential of 3.45 V. The current density measured is small in the potential range 0.0 to 1.0 V. From 1.0 V to 1.2 V a rapid rise in the current density is observed. The current within this potential region is associated with the formation of a porous InP layer [26–29]. The current density then continues to rise more slowly as the potential is further increased to 1.2 V where a maximum of 0.38 A cm^{-2} in the current density is reached. The current density decreases with further increases in potential up to 2.6 V where it increases abruptly. Well-defined current oscillations are observed in the potential range 2.6 V to 2.9 V and have an average current density of 0.35 A cm^{-2}. The current density versus potential curves were found to have a similar oscillatory region for all the scan rates investigated. Figure 1b is the voltammetric response of an n-InP electrode at a scan rate of 500 mV s^{-1}. As is obvious from comparing Fig. 1a and Fig. 1b, increasing the scan rate results in the shifting of the current-voltage response to more anodic potentials. In Fig. 1b the current oscillations now lie in the potential range 3.0 V to 3.3 V. Oscillations are also observed to always appear after the first primary anodic peak and lie in a potential window of $\sim$0.3 V. Furthermore, the average current density of the oscillations is observed to increase with increasing scan rate. Although not shown for clarity, anodization at lower scan rates results in a greater number of oscillations with lower average current density and they are observed at lower potentials.

Figure 2 shows the voltammetric response of similar electrodes at lower scan rates of

50 mV s^{-1} and 150 mV s^{-1}. As just previously mentioned, the primary anodic peak and subsequent current oscillations are observed at lower potentials. It is also observed that there is a significant increase in the number of oscillations at lower scan rates with correspondingly lower average current densities. As can be seen, at lower scan rates the characteristic current oscillations are preceeded by precursor oscillations that have a well defined shape and are only observed when the potential is scan at rates between 50 mV s^{-1} and 200 mV s^{-1}. The exact reason for the presence of these particular oscillations will be addressed in a future publication. The inset to Fig. 2 shows the current-voltage response at 600 mV s^{-1} where no characteristic oscillations are observed. Oscillations observed at such high scan rates are often random and irregular and show no obvious parameter dependencies. Under the experimental conditions outlined above, oscillations are not observed at scan rates below 50 mV s^{-1} nor are they observed at scan rates greater than 600 mV s^{-1}.

Figure 3 shows, on an expanded potential axis, the current oscillations shown in Fig. 1a. The current density of each oscillation increases with a progressively increasing slope up to a well-defined current maximum followed by a sharp decrease to a well-defined current minimum. The period segment τ_1 is defined to be the time taken for the current to increase from a minimum value to a maximum value during an oscillation. The period segment τ_2 is defined as the time taken for the current to decrease from a maximum to a minimum in current during an oscillation. The total period of oscillation is then $(\tau_1 + \tau_2)$. For the purposes of studying the potential dependence, we define the potential of an oscillation as the potential value at the current maximum for the oscillation.

The relationship of the values of τ_1, τ_2 and $(\tau_1 + \tau_2)$ to potential was investigated by plotting them against the applied potential and the results are plotted in this way in Fig. 4a. The total period of oscillation $(\tau_1 + \tau_2)$ is observed to increase linearly at a rate of 0.906

s V^{-1} as the potential is increased. The value of τ_1 is also found to increase linearly with applied potential. However, the value of τ_2 decreases slightly at a rate of 0.096 s V^{-1} as the applied potential increases. From Fig. 4a it is apparent that the total period of oscillation, and indeed one of its constituent parts τ_1, show a well defined strong dependence on the value of the potential, whereas the value of τ_2 is much less sensitive to the value of the applied potential. The charge passed during each oscillation was estimated by numerical integration of the current with respect to time. This estimation was done for each oscillation in a potential sweep at 100 mV s^{-1} (*i.e.* same data set as Fig. 4a). The charge per oscillation was plotted against the potential of the oscillation and a typical plot is shown in Fig. 4b. The charge associated with the segments τ_1 and τ_2 are also plotted (Q_1 and Q_2 respectively). As can be seen in Fig. 4b the total charge per cycle ($Q_1 + Q_2$) increases with increasing potential and a rate of approximately 0.268 C cm^{-2} V^{-1} was obtained from the slope of the linear fit to the data. The charge passed during the time segment τ_1 also increases linearly with increasing potential, whereas the charge passed during the time segment τ_2 decreases slightly as the potential increases. The segment, τ_1, is observed to represent the major portion of the total charge per cycle, whereas the charge associated with segment τ_2 is relatively constant with a measured decrease of 0.032 C cm^{-2} V^{-1}.

The charge per cycle was also estimated by numerical integration for the composite series of potential sweeps with scan rates in the range of 50 mV s^{-1} to 500 mV s^{-1}. Investigation of the oscillatory region of voltammograms acquired in this scan rate range revealed that the oscillation profile retains the same form as that shown in Fig. 1, regardless of the scan rate. This data was plotted as a function of the potential of oscillation. A strong linear dependence was observed as shown in Fig. 5. The slope of the linear fit yields a value of 0.216 C cm^{-2} V^{-1} for the increase in the charge per cycle with applied potential. It

was previously stated that, as the scan rate increases, the range of the oscillatory region is shifted to higher potentials. The composite data set (represented in Fig. 4a) therefore includes a larger overall range of potential and the charge per cycle is a well-behaved linear function of potential over this expanded range. Thus, for a particular scan rate, the period of oscillation decreases with increasing potential. Due to the fact that the average current density of each oscillation at a particular scan rate remains unchanged, it follows that the charge must increase with potential in a similar manner *i.e.* the rate of change of the charge per cycle as a function of potential is the product of the rate of change of the period with potential and the average current density of the oscillation.

Earlier reports of oscillations on InP in $(NH_4)_2S$ electrolytes showed that the charge per cycle remained approximately constant at $\sim$0.32 C cm^{-2} under potentiodynamic and potentiostatic conditions [19, 31]. Thus, while the observations in both systems are dissimilar in some regards, both show reproducible and well-behaved values of charge per cycle.

Oscillations in the current were also observed during potentiostatic conditions. A series of experiments were carried out in which the potential was stepped from open circuit to 1.7 V in a range of KOH electrolyte concentrations. Typical current-time curves are shown in Fig. 6 for electrodes anodized in 5 mol dm^{-3} and 3 mol dm^{-3} KOH respectively. It can be seen that asymmetrical oscillations are observed in both electrolytes, which die out very quickly. Fig. 7 shows the current-time curve of an InP electrode subjected to potentiostatic anodization in 2 mol dm^{-3} KOH under the same conditions to those described for Fig. 6. The oscillations are in marked contrast to those observed in higher KOH concentrations. Very reproducible sinusoidal oscillations of the current are observed which continue for much longer times than those in 5 mol dm^{-3} KOH as evident in Fig. 7. Numerical integration of the current with respect to time shows that a constant charge per cycle is maintained

during the oscillations. Furthermore, this trend is found to hold at higher potentials where the average current density of the oscillations is higher. The increase in the charge per cycle value is due to the increase in the period of oscillation as the potential is increased. In contrast to all observations in higher concentrations of KOH, no oscillations of any kind are found when InP electrodes are anodized in 1 mol dm^{-3} [26, 27]. Further work is required to elucidate this change and the results will be presented in a future publication, however, it is worth noting that in 1 and 5 mol dm^{-3} KOH porous In_2O_3 film growth occurs. Only when porous InP formation occurs are characteristic current oscillations observed concurrently.

Microscopic examination of electrodes subjected to potential sweep conditions such as those described for Fig. 1 showed that the current observed corresponds to complex anodic processes involving porous InP formation and anodic film formation. Figure 8a shows a bright field through focal TEM image of a sample which was anodized from 0.0 V to 2.35 V at a scan rate of 100 mV s^{-1}. Three distinct layers can be observed on the surface of the InP: an obviously porous or pitted layer at C next to the substrate D, an intermediate layer B and an outer porous layer A. TEM electron diffraction has been used to identify layers A and C as InP, and layer B as In_2O_3. Higher magnification TEM images (shown in the inset to Fig. 8a) reveal that the In_2O_3 layer appears to be nano-porous and also suggests that the layer labelled C in Fig. 8a is a pitted region of the InP substrate. Figure 8b shows a plan view SEM image of an InP electrode anodized under constant potential conditions at 1.7 V (SCE) for 43 s. It is noted that a thick, cracked anodic film has formed on the substrate, which itself is observed to be pitted, similar to that observed for layer C in Fig. 8a. This cracked and porous anodic layer on top of the pitted substrate surface is quite similar to layer B in Fig. 8a. The inset to Fig. 8b shows the same substrate and anodic film but with a segment of the porous InP layer (similar to layer A in Fig. 8a) also. This is direct evidence

that all three layers co-exist after anodization as separate entities. These observations are very similar to those observed under potential sweep conditions implying that the underlying mechanisms are quite similar. Thus, it appears that the pitting of the substrate (C) and growth of the In_2O_3 film (B) occurs during the potential region in which oscillations are observed.

Although the reason for the oscillatory behavior reported here is not yet known, comparison to the observations proposed by Lehmann [32], who suggest that the proposed mechanism for oscillatory behavior is pore formation and blocking, the observations reported here suggest that such a mechanism is in some way applicable. Indeed, microscopic examination of InP electrodes after anodization show that the current oscillations observed during anodization in the $(NH_4)_2S$ solution are accompanied by the growth and thickening of a porous In_2S_3 film with columnar structure [33]. However, TEM images of samples at potentials just prior to the onset of oscillations show clearly defined pitting of the InP substrate with columnar film growth occurring from the bottom of the pits [26]. A similar mechanism may operate in InP/KOH.

The exact mechanism governing the oscillatory behavior on InP in KOH is not yet convincingly resolved. For the anodic oscillatory behavior of InP electrodes in $(NH_4)_2S$, the current densities are relatively high in the region where oscillations are observed and consequently, relatively large changes in the composition within the pores in the vicinity of the InP/film interface are expected. For example, anodic dissolution of InP is accompanied by H^+ formation and so significant changes in pH are expected. Similarly, the formation of In^{3+} and oxy-anions of phosphorous occurs and water may even be depleted. Under such conditions, the nucleation and growth of an insoluble phase at the interface would not be too surprising, which could cyclically inhibit faradaic processes at the interface. As already

pointed out by several authors [34, 35], the transport of ions through the oxide layer is a key to the understanding of the oscillatory phenomenon and it is possible that it could constitute the feedback mechanism, which is a requirement for an oscillatory system. The feedback mechanism may consist of a cyclic relaxation of the concentration gradients within the pores as the current decreases. This mechanism may allow dissolution of a thin oxide at the interface, which then allows current to flow again, resulting in the re-establishment of a high concentration gradient or re-formation of the thin oxide film.

Based on these hypotheses and the microscopic examination of the electrodes at various points during the oscillatory regime, we propose the following mechanism for the observed current oscillations on InP under anodic conditions. As already presented in Fig. 8, the surface of the InP beneath the porous In_2O_3 layer has a pitted morphology. We suggest that the current oscillations reflect the cyclical variation of the geometry (surface area) of this interface with time. Figure 9 shows TEM micrographs of electrodes prior to oscillations (Fig. 9a) and also after anodization to an oscillation minimum (Fig. 9b). The micrographs clearly show that prior to oscillations, a porous InP layer is formed and the InP interface can be seen to have an undulating morphology consistent with preferential etching. As shown in Fig. 8, the result of the oscillation current is that the InP interface becomes pitted in a relatively regular manner. At an oscillation current minimum, it can be observed from Fig. 9b that the InP interface is relatively planar. We can thus infer from these observations that the current density at an oscillation minimum is due to a minimum in InP surface area. After a very brief recovery-induction period, the current begins to increase again, pitting of the InP interface occurs and as a result the current increases. The pits on the InP surface continue to develop until the maximum in current density is reached, after which the delamination of these pitted structures is observed (see Fig. 8a). This lift-off or undercutting

continues to occur and as a result the active geometric surface of the InP becomes minimal with time until the current minimum is again reached and the surface is observed to be devoid of U-shaped pitted structures.

This mechanism can be qunatitavively validated by estimating charge per cycle at the potential at which the anodization was stopped for microscopic examination and thus determining the associated thickness of InP removed. This quantity can then be compared to the measured InP removed during the oscillation cycle in question. Using Faraday's law, the thickness d of InP oxidized to the charge density Q is given by the equation,

$$d = \frac{V_{M(InP)}Q}{nF} \tag{1}$$

where d is the etch depth, $V_{M(InP)}$ is the molar volume of InP, F is the Faraday constant and n is the number of electrons transferred per formula unit of InP. The estimated charge accumulated during the oscillation cycles where the microscopic examination was performed is 0.216 C cm^{-2} V^{-1}. Values of etch depth were estimated in this way using a value [36] of 30.31 cm^3 for $V_{M(InP)}$ and assuming an electrochemical process such as

$$2InP + 22OH^- \rightarrow In_2O_3 + 2PO_4^{3-} + 11H_2O + 16e^- \tag{2}$$

leading to the formation of partially soluble In_2O_3 and dissolved oxo-anions of phosphorous. The formation of PO_4^{3-} (a P^V oxo-anion) as written corresponds to an $n = 8$-electron (per InP) process. A theoretical value of ~85 nm V^{-1} is estimated from Eqn. (1) for d, the etch depth assuming complete removal of InP per unit charge passed. Thus the theoretical value is in reasonable agreement with the measured depth of the pitted structures by TEM (70 - 100 nm) indicating that the electrochemical and microscopic measurments are somewhat consistent. Thus, the reason and result of electrochemical current ocillations on InP is certainly semi-quantitatively explicable by the proposed mechanism.

It has been observed experimentally [37] that below a threshold electrolyte concentration of $\sim$1.5 mol dm^{-3} KOH porous InP growth does not occur and instead the formation of oxide films on the InP surface is observed. Once the electrolyte concentration drops below this threshold concentration, the result is the coincidental thickening of the porous In_2O_3 film above the InP surface. Recovery of the electrolyte concentration is quite rapid and further thickening of the anodic film occurs due to a dissolution-reprecipitation mechanism during the oscillatory cycles.

It is apparent, however, that the oscillations reported here are governed by a fairly robust mechanism, which results in very reproducible behavior. Thus, for example, the charge per cycle increases linearly with potential for potentiodynamic experiments and remains constant for potentiostatic experiments. Although it is possible that the oscillations are due to large changes in composition, including concurrent solid film formation and electrolyte depletion, it is the cyclical pitting dissolution and resulting effective surface area variation of the InP that contributes predominantly to the measured current during the oscillatory cycles.

IV. CONCLUSIONS

In conclusion, well defined oscillations are observed during linear potential sweeps of InP in 5 mol dm^{-3} KOH to potentials above $\sim$1.7 V at scan rates in the range 50 mV s^{-1} to 500 mV s^{-1}. The oscillations observed exhibit an asymmetrical current versus potential profile. The rise time τ_1 of the oscillatory cycle shows a clear dependence on the potential whereas the fall time τ_2 is almost independent of potential. The charge associated with segment τ_1 is observed to represent the major portion of the total charge per cycle and this increases with increasing potential. It is very clear that the charge per cycle is a very well-behaved function of potential and increases with a linear dependence. Oscillations are also observed

under potentiostatic conditions with assymetric-damped oscillations observed in the higher KOH concentrations and relatively symmetrical sinusoidal oscillations observed in 2 mol dm^{-3} KOH.

Current oscillations on n-InP anodes are observed to be very sensitive to carrier concentration and electrolyte concentration. Oscillations are observed under constant potential and potential sweep conditions in 5, 3 and 2 mol dm^{-3} KOH, but not in 1 mol dm^{-1} KOH. Furthermore, electrodes with doping densities below $\sim 10^{18}$ cm^{-3} do not undergo any oscillatory behavior irrespective of the anodization conditions or electrolyte concentration.

Cross-sectional TEM analysis of post-anodization electrodes suggest that the oscillations are linked to cyclical changes in the surface area of the InP surface. At the current maximum of an oscillation, a relatively higher surface area pitted surface is observed whereas at a current minimum a planar featureless surface is noted. Thus we propose a mechanism whereby the oscillations are controlled by cyclical alterations to the geometrical morphology of the InP surface with time.

Acknowledgements

One of the authors (CO'D) wishes to acknowledge the financial support of an Enterprise Ireland Postdoctoral Scholarship.

[1] Russell, P.; Newman, J. *J. Electrochem. Soc.* **1986**, *133*, 2093.

[2] Beck, T. R. *J. Electrochem. Soc.* **1982**, *129*, 2412.

[3] Sazou, D. *Electrochim. Acta* **1997**, *42*, 627.

[4] Glarum, S. H.; Marshall, J. H. *J. Electrochem. Soc.* **1985**, *132*, 2827.

[5] Bassett, M. R.; Hudson, J. L. *J. Electrochem. Soc.* **1990**, *137*, 922.

[6] Hudson, J. L.; Tsotsis, T. T. *Chem. Eng. Sci.* **1994**, *49*, 1493.

[7] Blackwood, D. J.; Borazio, A.; Greef, R.; Peter, L. M.; Stumper, J. *Electrochim. Acta* **1992**, *37*, 889.

[8] Cattarin, S.; Decker, F.; Dini, D. *J. Phys. Chem. B* **1998**, *102*, 4779.

[9] Dini, D.; Cattarin, S.; Decker, F. *J. Electroanal. Chem.* **1998**, *466*, 7.

[10] Chazalviel, J.-N.; Ozanam, F.; Etman, M.; Paolucci, F.; Peter, L. M.; Stumper, J. *J. Electroanal. Chem.* **1992**, *327*, 343.

[11] Aggour, M.; Giesig, M.; Lewerenz, H. J. *J. Electroanal. Chem.* **1995**, *383*, 67.

[12] Carstensen, J.; Prange, R.; Föll, H. *J. Electrochem. Soc.* **1999**, *146*, 1134.

[13] Rauscher, S.; Dittrich, Th.; Aggour, M.; Rappich, J.; Flietner, H.; Lewerenz, H. J. *Appl. Phys. Lett.* **1995**, *66*, 22.

[14] Stumper, J.; Greef, R.; Peter, L. M. *J. Electroanal. Chem.* **1991**, *310*, 445.

[15] Parkhutik, V. *Solid State Electron.* **2001**, *45*, 1451.

[16] Parkhutik, V. *Mater. Sci. Eng. B* **2002**, *88*, 269.

[17] Lewerenz, H. J.; Aggour, M. *J. Electroanal. Chem.* **1993**, *351*, 159.

[18] Parkhutik, V.; Matveeva, E.; Perez, R.; Alamo, J.; Beltran, D. *Mater. Sci. Eng. B* **2000**,

69-70, 553.

[19] Harvey, H.; Buckley, D. N. *Electrochem. Solid-State Lett.* **2002**, *5*, G22.

[20] Buckley, D. N.; Harvey, E.; Chu, S. N. G. in *Proceedings of the State-of-the-Art Program on Compound Semiconductors XXXVI and Wide Bandgap Semiconductors for Photonic and Electronic Devices and Sensors III*, Kopf, R. F.; Ren, F.; Stokes, E. B.; Ng, H. M.; Baca, A. G.; Pearton, S. J.; Chu, S. N. G. Editors, **2002**, *PV 2002-3*, 286, The Electrochemical Society, Proceedings Series, Pennington, NJ.

[21] Langa, S.; Carstensen, J.; Tiginyanu, I. M.; Christophersen, M.; Föll, H. *Electrochem. Solid-State Lett.* **2001**, *4*, G50.

[22] Schmuki, P.; Schlierf, U.; Herrmann, T.; Champion, G. *Electrochimica Acta* **2003**, *48*, 1301.

[23] Tsuchiya, H.; Hueppe, M.; Djenizian, T.; Schmuki, P. *Surf. Sci.* **2003**, *547*, 268.

[24] Hamamatsu, A.; Kaneshiro, C.; Fujikura, H.; Hasegawa, H. *J. Electroanal. Chem.* **1999**, *473* 223.

[25] Giannuzzi, L. A.; Stevie, F. A. *Micron.* **1999**, *30*, 197.

[26] Harvey, E.; O'Dwyer, C.; Melly, T.; Buckley, D. N.; Cunnane, V. J.; Sutton, D.; Newcomb, S. B.; Chu, S. N. G. in *Proceedings of the State-of-the-Art Program on Compound Semiconductors XXXV*, Chang, P.C.; Chu, S. N. G.; Buckley, D. N. Editors, **2001**, *PV 2001-20*, 87, The Electrochemical Society, Proceedings Series, Pennington, NJ.

[27] O'Dwyer, C.; Buckley, D. N.; Cunnane, V. J.; Sutton, D.; Serantoni, M.; Newcomb, S. B. in *Proceedings of the State-of-the-Art Program on Compound Semiconductors XXXVII*, Chang, P.-C.; Chan, W. K.; Buckley, D. N.; Baca, A. G. Editors, **2002**, *PV 2002-14*, 259, The Electrochemical Society, Proceedings Series, Pennington, NJ.

[28] O'Dwyer, C.; Buckley, D. N.; Sutton, D.; Newcomb, S. B. in *Proceedings of the State-of-the-*

Art Program on Compound Semiconductors XXXVIII, Stokes, E. B.; Fitch, R. C.; Buckley, D. N.; Chang, P.-C.; Koide, Y.; Kopf, R. F. Editors, **2003**, *PV 2003-04*, 63, The Electrochemical Society, Proceedings Series, Pennington, NJ.

[29] Buckley, D. N.; O'Dwyer, C.; Harvey, E.; Melly, T.; Sutton, D.; Newcomb, S. B. (invited) in *Proceedings of the State-of-the-Art Program on Compound Semiconductors XXXVIII*, Stokes, E. B.; Fitch, R. C.; Buckley, D. N.; Chang, P.-C.; Koide, Y.; Kopf, R. F. Editors, **2003**, *PV 2003-04*, 48, The Electrochemical Society, Proceedings Series, Pennington, NJ.

[30] O'Dwyer, C.; Melly, T.; Harvey, E.; Buckley, D. N.; Cunnane, V. J.; Sutton, D.; Newcomb, S. B. in *Proceedings of the State-of-the-Art Program on Compound Semiconductors XXXVII*, Chang, P.-C.; Chan, W. K.; Buckley, D. N.; Baca, A. G. Editors, **2002**, *PV 2002-14*, 275, The Electrochemical Society, Proceedings Series, Pennington, NJ.

[31] Buckley, D. N.; Harvey, E.; Chu, S. N. G. *Monatshefte für Chimie* **2002**, *133*, 785.

[32] Lehmann, V. *J. Electrochem. Soc.* **1996**, *143*, 1313.

[33] Harvey, E.; Buckley, D. N.; Chu, S. N. G.; Sutton, D.; Newcomb, S. B. *J. Electrochem. Soc.* **2002**, *149*, B398.

[34] Gerischer, H.; Lübke, M. *Ber. Bunsen-Ges. Phys. Chem.* **1988**, *92*, 573.

[35] Chazalviel, J.-N. *Electrochim. Acta.* **1992**, *37*, 865.

[36] Cotton, F. A.; Wilkinson, G.; Murillo, C. A.; Bochmann, M. *Advanced Inorganic Chemistry* **1999**, John Wiley & Sons, New York.

[37] Lynch, R.; O'Dwyer, C.; Clancy, I.; Corcoran, D.; Buckley, D. N. in *Proceedings of the State-of-the-Art Program on Compound Semiconductors XLI*, Baca, A. G.; Chan, W. K.; Shiojima, K.; Kopf, R. F. Editors, **2004**, *PV 2004-6*, 85, The Electrochemical Society, Proceedings Series, Pennington, NJ.

Figure captions

Fig.1

Current density versus applied potential curves for n-InP electrodes in 5 mol dm^{-3} aqueous KOH at room temperature. The potential was scanned at (a) 300 mV s^{-1} and (b) 500 mV s^{-1} from 0.0 V to 3.45 V.

Fig.2

Current density versus applied potential curves for n-InP electrodes in 5 mol dm^{-3} aqueous KOH at room temperature. The potential was scanned at (a) 50 mV s^{-1} and (b) 150 mV s^{-1} from 0.0 V to 2.5 V. *inset* Current density versus applied potential curve when InP is anodized at a scan rate of 600 mV s^{-1} in 5 mol dm^{-3} KOH. No regular oscillations are observed.

Fig.3

Typical current oscillations observed during anodization of n-InP at a scan rate of 100 mV s^{-1} in 5 mol dm^{-3} KOH. The potential axis has been expanded for clarity in the figure. The characteristic period segments τ_1 and τ_2 are shown.

Fig.4

(a) Variation of τ_1, τ_2 and $(\tau_1 + \tau_1)$ as a function of oscillation potential. The data was acquired from a linear potential sweep at a scan rate of 100 mV s^{-1}. (b) Variation of the total charge per cycle $(Q_1 + Q_2)$, charge associated with time τ_1 (Q_1) and charge associated with τ_2 (Q_2), as a function of potential.

Fig.5

Total charge per cycle plotted as a function of potential. The data was acquired from potential sweeps of n-InP in 5 mol dm^{-3} KOH with scan rates in the range 50 mV s^{-1} to 500 mV s^{-1}.

Fig.6

Current-time curves for InP electrodes anodized at 1.7 V in (−) 5 mol dm^{-3} KOH and (···) 3 mol dm^{-3} KOH electrolytes. The data was acquired at room temperature in dark conditions.

Fig.7

Current-time curve for an InP electrode anodized at 1.7 V in 2 mol dm^{-3} KOH. The data was acquired at room temperature in dark conditions. The insert is an expanded view showing the oscillatory profile.

Fig.8

(a) Bright field through focal TEM image of an n-InP electrode after anodization from 0.0 V to 2.35 V (SCE) at a rate of 200 mV s^{-1} and a Pt layer is indicated which was deposited to prevent ion image to the underlying material during the preparation of the TEM sample. Four distinct layers are marked at A, B, C and D. *inset* Higher resolution TEM image showing the porosity of the In_2O_3 layer and the U-shaped pitted structure of the InP surface. (b) Plan view SEM image of InP electrode anodized at 1.7 V (SCE) in 5 mol dm^{-3} KOH. *inset* Section of same surface where the uppermost InP porous can also be observed.

Fig.9

(a) Bright field through focal TEM image of an n-InP electrode after anodization from 0.0 V to 1.6 V (SCE) at a rate of 200 mV s^{-1}. A porous InP layer is observed with a non-planar interface. (b) Dark field TEM micrograph of the InP electrode after anodization to 2.3 V (final current minimum).

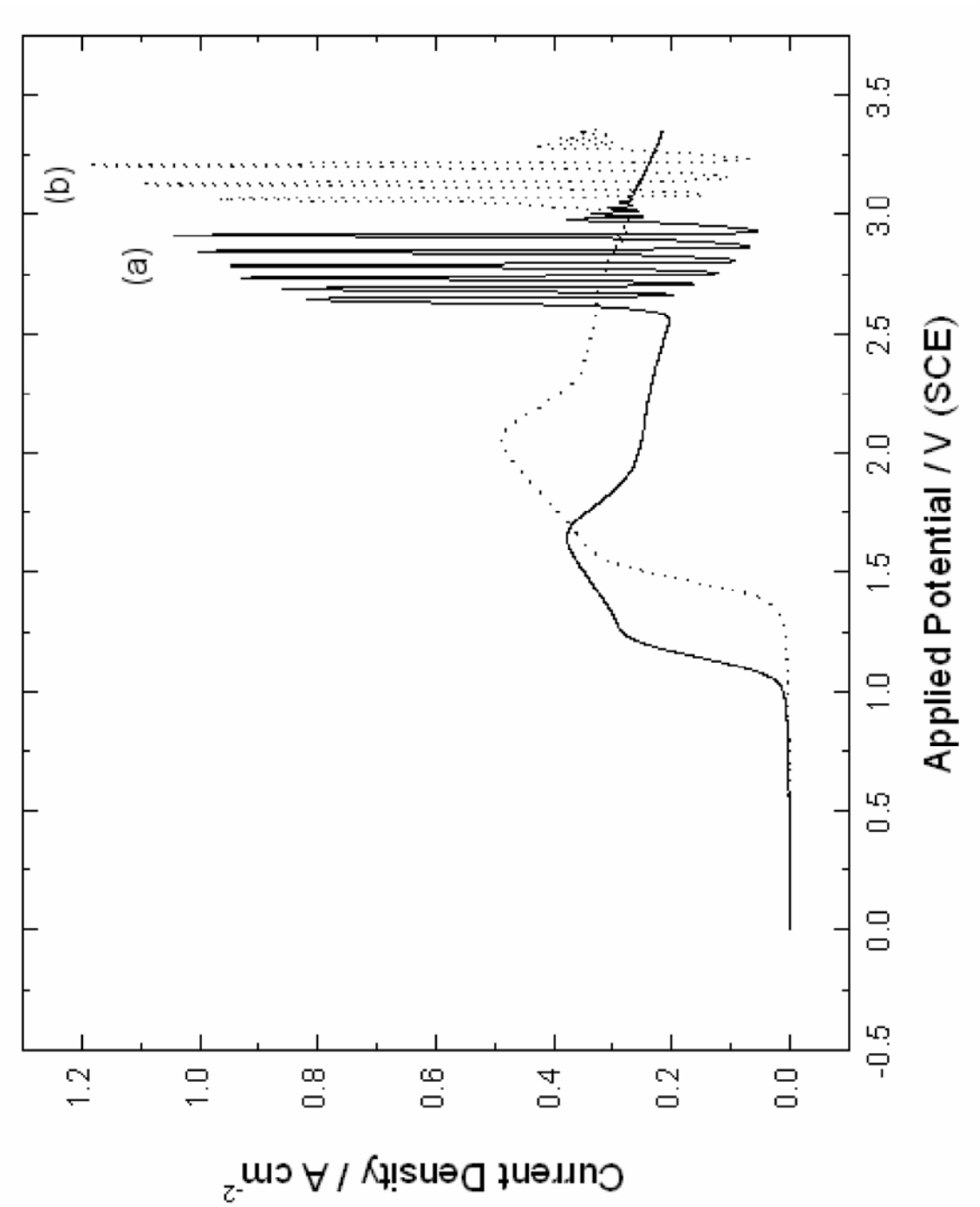
(a)
(b)
Applied Potential / V (SCE)
Current Density / A cm-2
-0.5
0.0
0.5
1.0
1.5
2.0
2.5
3.0
3.5
0.0
0.2
0.4
0.6
0.8
1.0
1.2

Fig. 1

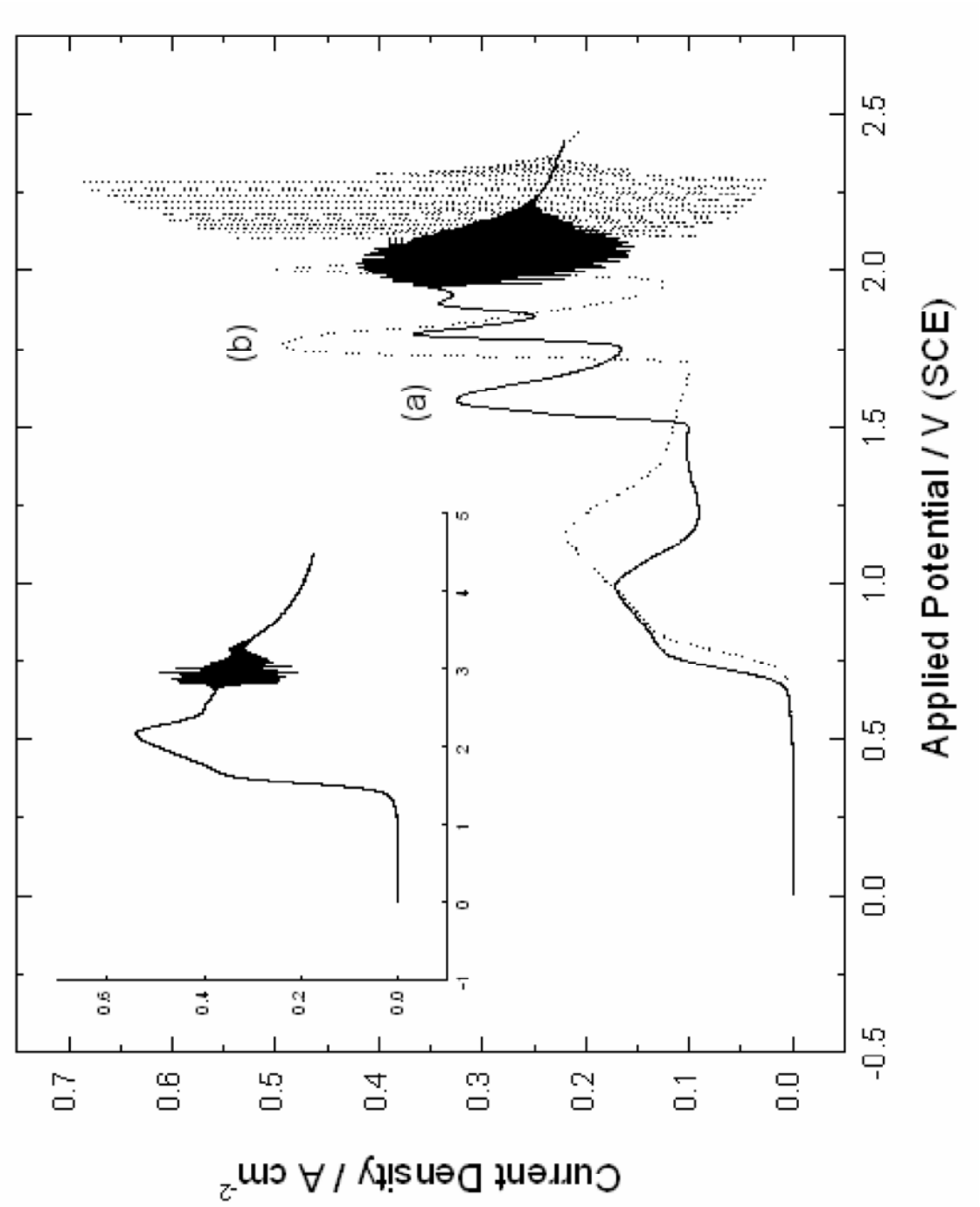

Fig. 2

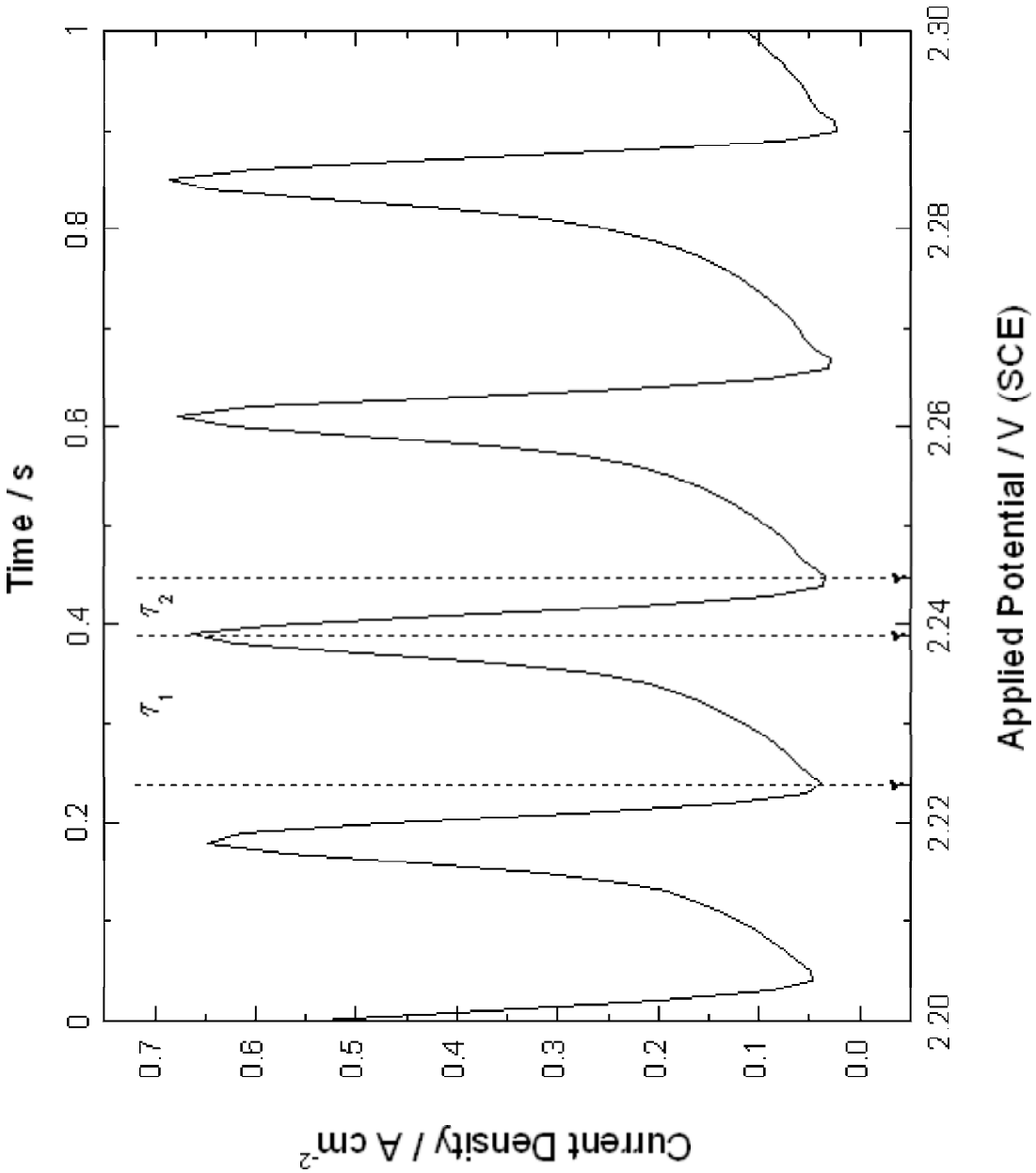
Time / s
Applied Potential / V (SCE)
Current Density / A cm-2
τ1
τ2
0
0.2
0.4
0.6
0.8
1
2.20
2.22
2.24
2.26
2.28
2.30
0.0
0.1
0.2
0.3
0.4
0.5
0.6
0.7

Fig. 3

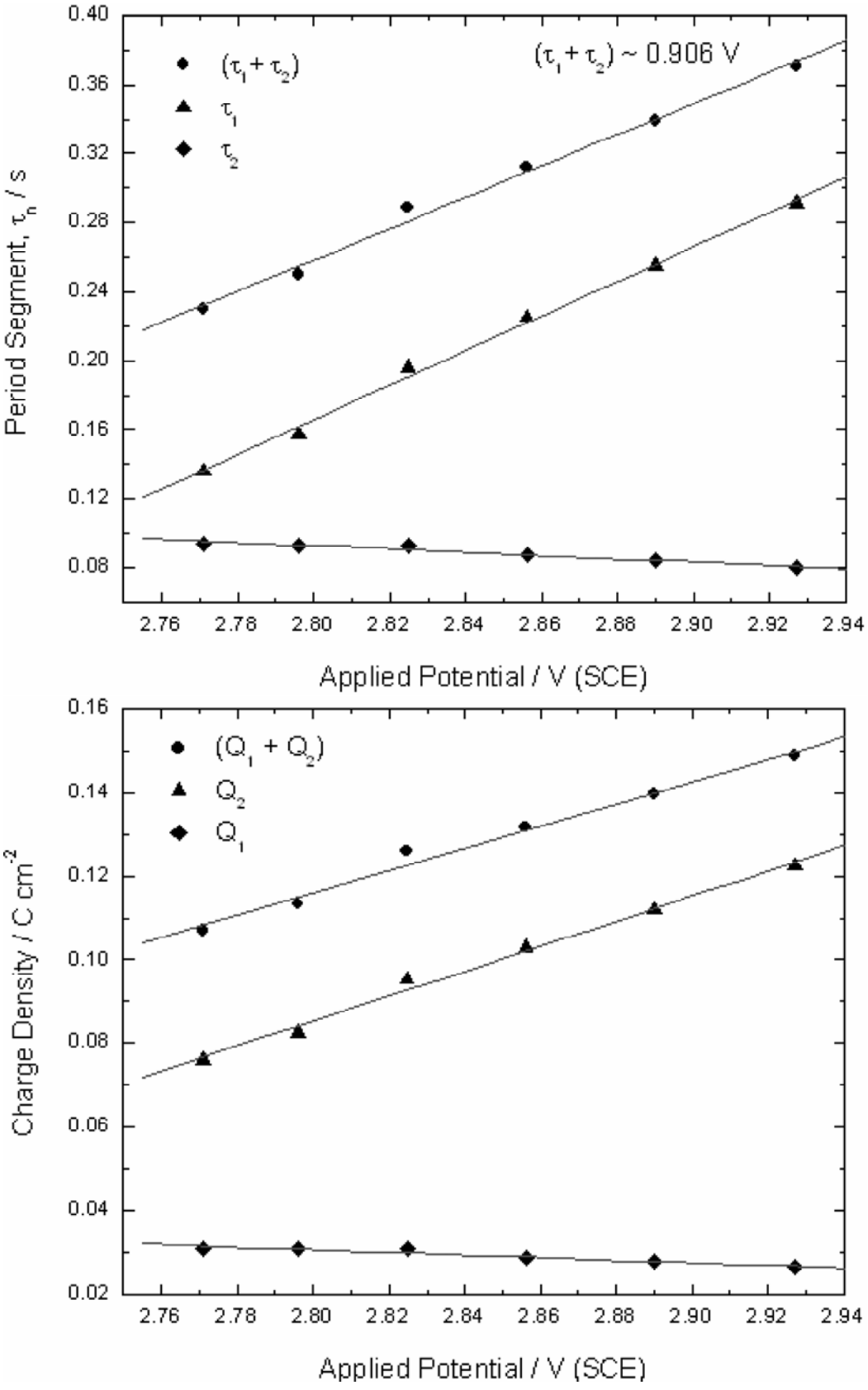
Period Segment, τ_n / s
$(\tau_1 + \tau_2)$
τ_1
τ_2
$(\tau_1 + \tau_2) \sim 0.906$ V
Applied Potential / V (SCE)
Charge Density / C cm^{-2}
$(Q_1 + Q_2)$
Q_2
Q_1
Applied Potential / V (SCE)

Fig. 4

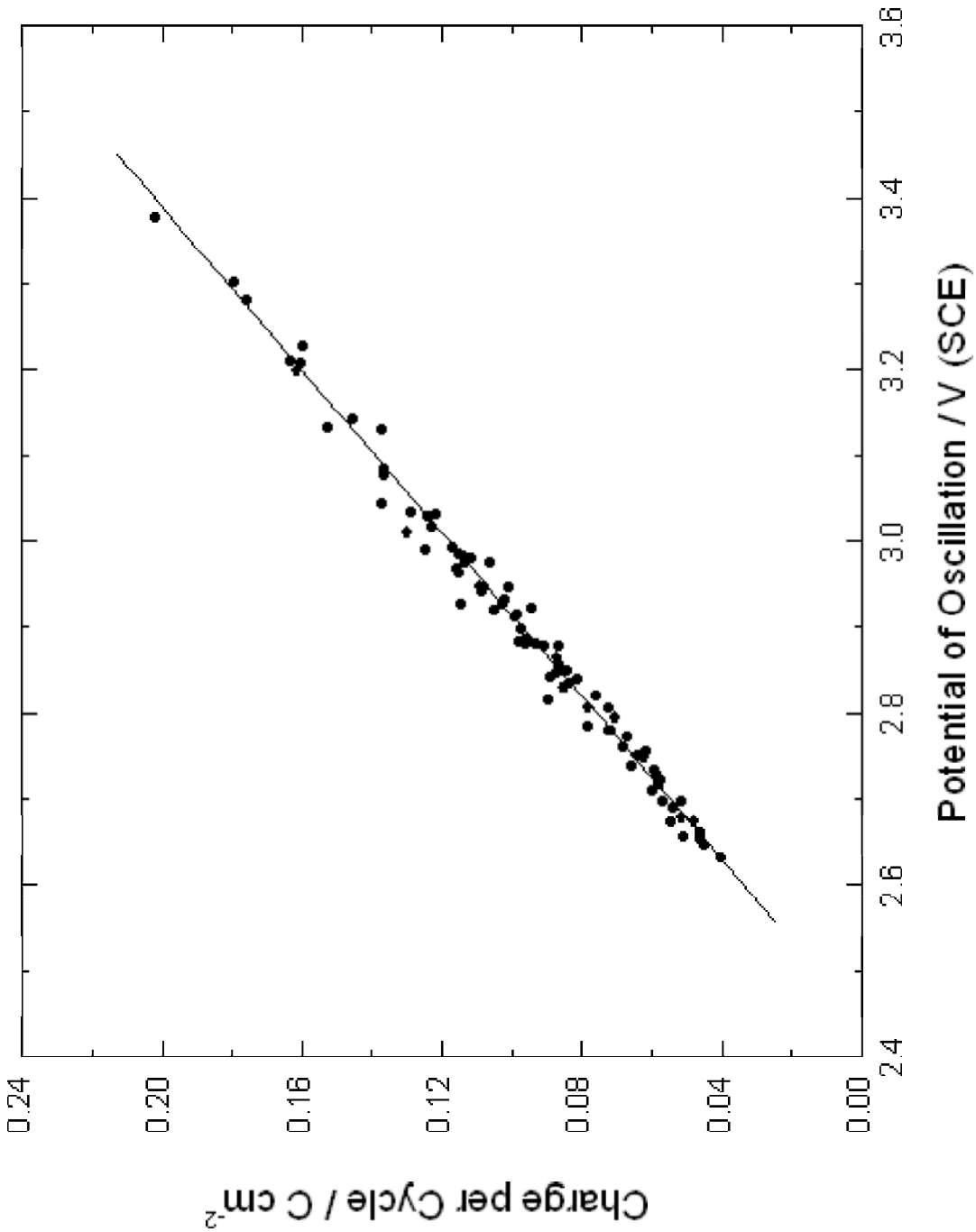
Charge per Cycle / C cm-2
0.00
0.04
0.08
0.12
0.16
0.20
0.24
Potential of Oscillation / V (SCE)
2.4
2.6
2.8
3.0
3.2
3.4
3.6

Fig. 5

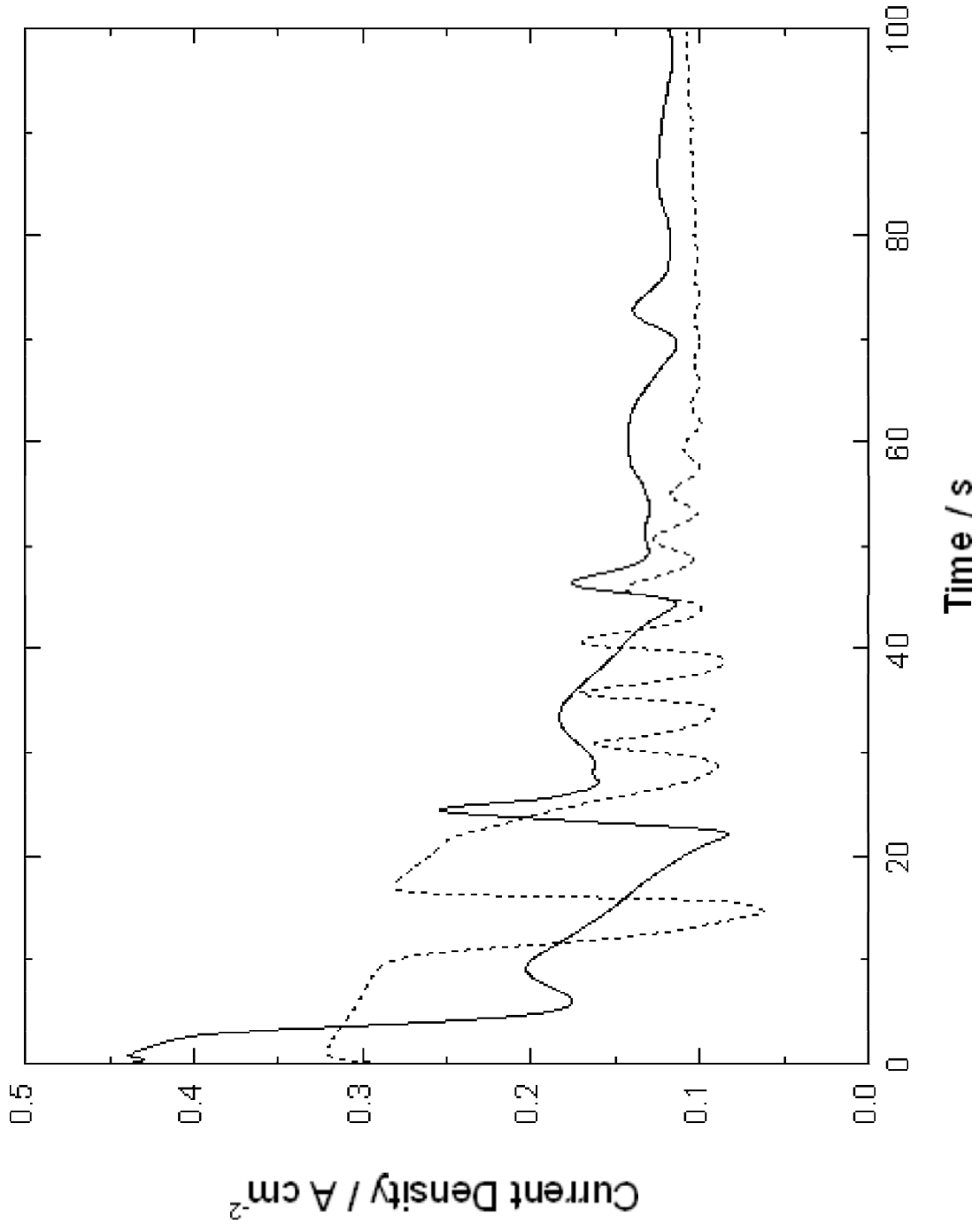

Fig. 6

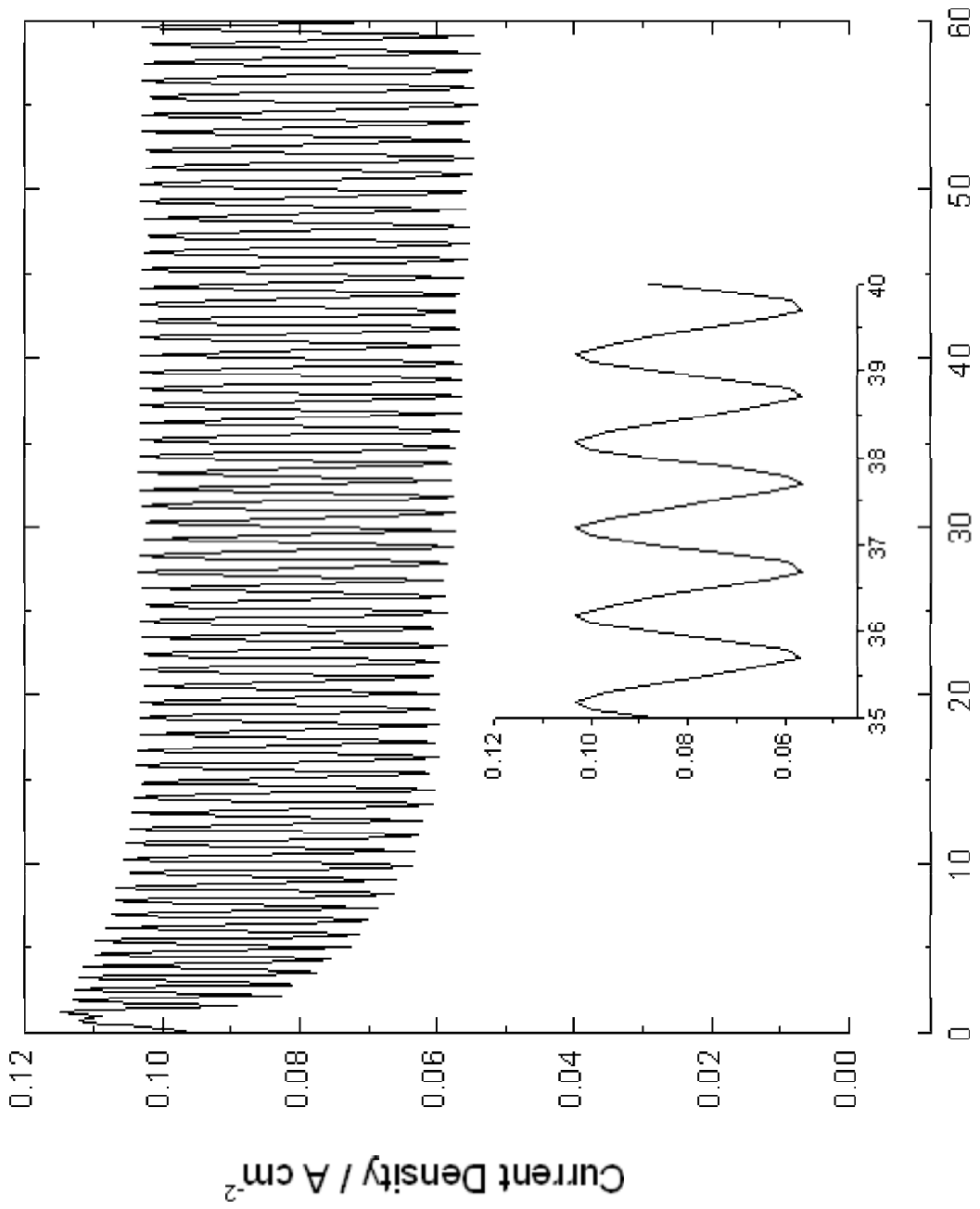
Current Density / A cm-2
0.12
0.10
0.08
0.06
0.04
0.02
0.00
0
10
20
30
40
50
60
Time / s
0.12
0.10
0.08
0.06
35
36
37
38
39
40

Fig. 7

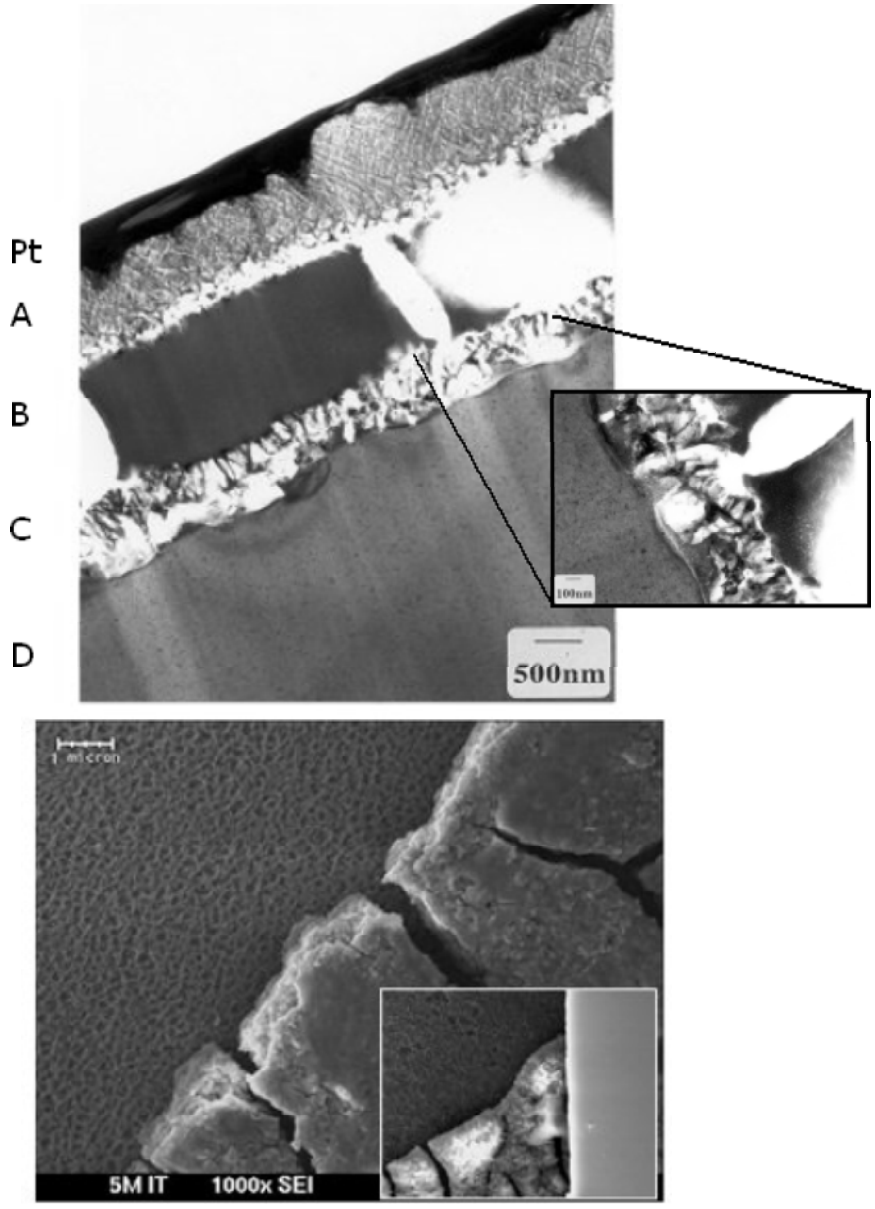

Fig. 8

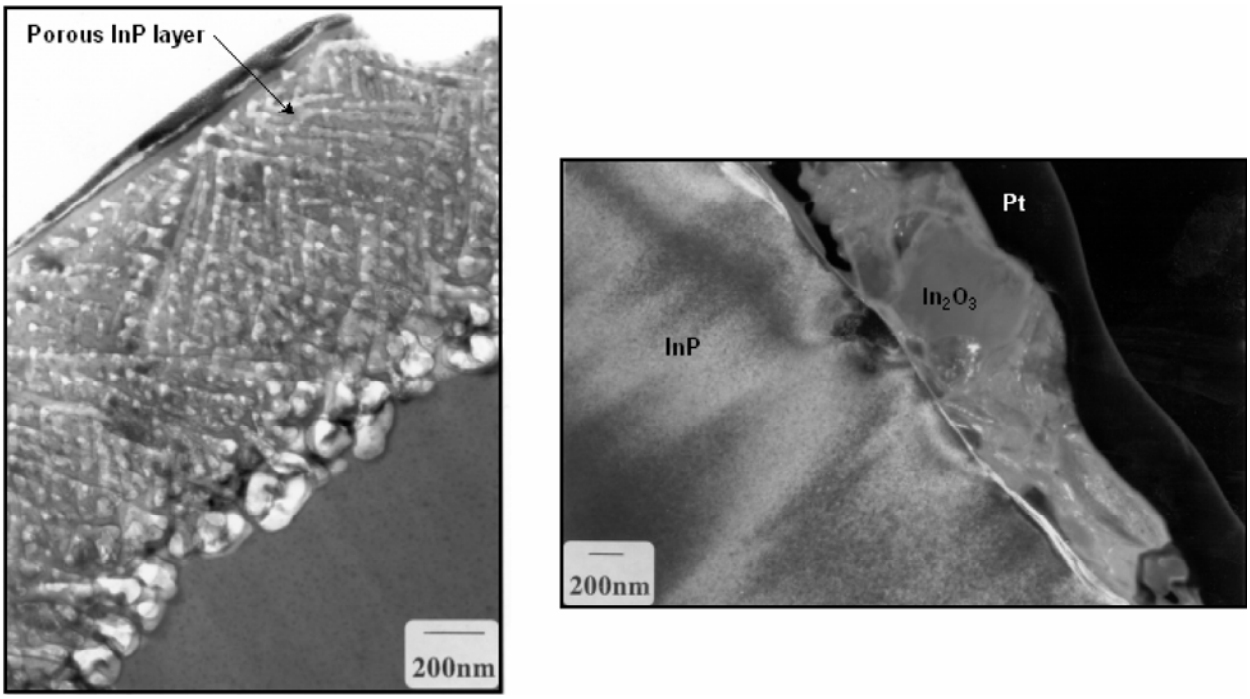

Fig. 9